

## **TITLE PAGE**

### **Starting currents of modes in cylindrical cavities with mode-converting corrugations for second-harmonic gyrotrons**

Tetiana I. Tkachova<sup>1</sup> (0000-0002-4605-3429)  
Vitalii I. Shcherbinin<sup>1,2\*</sup> (0000-0002-9879-208X)  
Viktor I. Tkachenko<sup>1,3</sup> (0000-0002-1108-5842)  
Zisis C. Ioannidis<sup>2</sup> (0000-0002-1233-9111)  
Manfred Thumm<sup>2,4</sup> (0000-0003-1909-3166)  
John Jelonnek<sup>2,4</sup> (0000-0002-0531-7600)

<sup>1</sup>National Science Center "Kharkiv Institute of Physics and Technology", 61108 Kharkiv, Ukraine

<sup>2</sup>Institute for Pulsed Power and Microwave Technology, Karlsruhe Institute of Technology, 76131 Karlsruhe, Germany

<sup>3</sup>V.N. Karazin Kharkiv National University, 61022 Kharkiv, Ukraine

<sup>4</sup>Institute of Radio Frequency Engineering and Electronics, Karlsruhe Institute of Technology, 76131 Karlsruhe, Germany

\*e-mail: vshch@ukr.net

**Abstract** A self-consistent system of equations (known as single-mode gyrotron equations) is extended to describe the beam-wave interaction in a cylindrical gyrotron cavity with mode-converting longitudinal corrugations, which produce coupling of azimuthal basis modes. The system of equations is applied to investigate the effect of corrugations on starting currents of the cavity modes. For these modes, eigenvalues, ohmic losses, field structure and beam-wave coupling coefficients are investigated with respect to the corrugation parameters. It is shown that properly-sized mode-converting corrugations are capable of improving the selectivity properties of cylindrical cavities for second-harmonic gyrotrons.

**Keywords** gyrotron, corrugated cavity, starting current, mode conversion, cyclotron harmonic

#### **Declarations**

**Funding** Partial financial support was received from the Alexander von Humboldt Foundation.

**Conflicts of interest/Competing interests** The authors have no conflicts of interest to declare that are relevant to the content of this article.

**Ethics approval** Not applicable

**Consent to participate** Not applicable

**Consent for publication** Not applicable

**Availability of data and material** Data are available from the authors upon reasonable request.

**Code availability** Not applicable

**Authors' contributions** All authors contributed to the study conception and design. Material preparation, data collection and analysis were performed by Tetiana I. Tkachova and Vitalii I. Shcherbinin. The first draft of the manuscript was written by Vitalii I. Shcherbinin and all authors commented on previous versions of the manuscript. All authors read and approved the final manuscript.

# Starting currents of modes in cylindrical cavities with mode-converting corrugations for second-harmonic gyrotrons

Tetiana I. Tkachova<sup>1</sup>, Vitalii I. Shcherbinin<sup>1,2\*</sup>, Viktor I. Tkachenko<sup>1,3</sup>, Zisis C. Ioannidis<sup>2</sup>, Manfred Thumm<sup>2,4</sup>, and John Jelonnek<sup>2,4</sup>

<sup>1</sup>National Science Center "Kharkiv Institute of Physics and Technology", 61108 Kharkiv, Ukraine

<sup>2</sup>Institute for Pulsed Power and Microwave Technology, Karlsruhe Institute of Technology, 76131 Karlsruhe, Germany

<sup>3</sup>V.N. Karazin Kharkiv National University, 61022 Kharkiv, Ukraine

<sup>4</sup>Institute of Radio Frequency Engineering and Electronics, Karlsruhe Institute of Technology, 76131 Karlsruhe, Germany

\*e-mail: vshch@ukr.net

**Abstract** A self-consistent system of equations (known as single-mode gyrotron equations) is extended to describe the beam-wave interaction in a cylindrical gyrotron cavity with mode-converting longitudinal corrugations, which produce coupling of azimuthal basis modes. The system of equations is applied to investigate the effect of corrugations on starting currents of the cavity modes. For these modes, eigenvalues, ohmic losses, field structure and beam-wave coupling coefficients are investigated with respect to the corrugation parameters. It is shown that properly-sized mode-converting corrugations are capable of improving the selectivity properties of cylindrical cavities for second-harmonic gyrotrons.

**Keywords** gyrotron, corrugated cavity, starting current, mode conversion, cyclotron harmonic

## 1. Introduction

Second-harmonic gyrotrons with available superconducting magnets are currently the most powerful sources of coherent continuous-wave radiation for a wide variety of emerging applications in sub-terahertz-to-terahertz frequency range [1, 2]. One of the main factors limiting their performance is the competition from the first-harmonic modes, which can be explained by the fact that starting currents of the first-harmonic modes are naturally much lower than those of the second-harmonic modes. This feature is described by the simple approximate formula [3, 4]

$$\frac{I_1}{I_2} \approx 4\beta_{\perp 0}^2 \frac{Q_2}{Q_1} \left( \frac{L_2}{L_1} \right)^2 \frac{C_{m,2}^2}{C_{l,1}^2} \quad (1)$$

where  $I_s$ ,  $Q_s$ ,  $L_s$  and  $C_{m,s}^2$  are the minimum starting current, total quality factor, effective cavity length and beam-wave coupling coefficient for the  $s$ -th harmonic  $TE_{m,p}$  mode interacting with a helical electron beam in a gyrotron cavity, respectively,  $\beta_{\perp 0} = \sqrt{(1-\gamma_0^{-2})/(1+\alpha^{-2})}$  is the initial transverse electron velocity normalized to the speed of light in vacuum,  $\gamma_0$  and  $\alpha$  are the initial relativistic and pitch factors of the electrons, respectively.

In gyrotrons with conventional cylindrical cavities,  $L_1 \approx L_2$  and the ratio  $Q_2/Q_1$  of total quality factors can approach the peak value of 4 [5], provided that the ohmic losses in metal cavity walls are negligible. Despite this, the minimum starting currents of the first-harmonic modes are usually several times lower than those of the second-harmonic modes [3, 6-11]. The main reason lies in the constraint  $\beta_{\perp 0}^2 \ll 1$  for conventional weakly-relativistic gyrotrons [3, 4]. This constraint is inevitable and becomes more rigid for lower beam voltages. An additional limiting factor is associated with the ratio  $C_{m,2}^2/C_{l,1}^2$ . This ratio is often distinctly smaller than unity, since the peak values of the beam-wave coupling coefficients of the first-harmonic modes are generally several times those of the second-harmonic modes. Besides, in low-power second-harmonic gyrotrons with broadband continuous frequency tuning, long cavities are employed to reduce the operating beam current and to provide continuous transition between high-order axial modes [3, 12-15]. In such cavities, the contribution of ohmic wall losses to the total quality factor is large [16]. It reduces the value of  $Q_2/Q_1$ , thereby providing further decrease in the ratio  $I_1/I_2$  of starting currents of the first- and second-harmonic modes. Because of the small ratio  $I_1/I_2$ , operation of low-current second-harmonic gyrotrons equipped with conventional cavities requires careful choice of the operating mode, which must be well-isolated in frequency from dangerous first-harmonic competitors. As the oscillation frequency and eigenvalue of the operating mode increase, it becomes more and more difficult to fulfill this requirement.

This brings to the forefront the need for the use of advanced cavities with improved mode selection in sub-terahertz and terahertz second-harmonic gyrotrons. Among them are cavities enabling selective decrease of diffraction losses of the operating second-harmonic modes, with a consequent increase of the ratios  $Q_2/Q_1$  and  $I_1/I_2$  in (1). Such cavities include iris-loaded cavities [17, 18], coaxial cavities with tapered corrugated [19] or smooth [9] inserts, cavities with output reflectors [20], cavities with distributed dielectric coating [21] or impedance corrugations [22]. However, ohmic wall losses substantially reduce the benefit from using these cavities in low-power second-harmonic gyrotrons. Better performance can be theoretically achieved in coaxial gyrotron cavities with resistive inserts [19, 23], which make it possible to increase the ohmic losses of competing modes. However, their chief practical drawback is the very low conductivity required for resistive (conducting) rods to ensure efficient suppression of high-order axial modes, which often brings the major threat to operation of second-harmonic gyrotrons [6-11] and feature high diffraction losses. Such conductivity can be beyond the

range of the available metallic materials, especially in the terahertz range [11]. For mode selection by ohmic losses, dielectric inserts made from available lossy ceramics can be used as alternative to resistive rods in cavities of sub-terahertz second-harmonic gyrotrons [11]. In practice, such a use would require further research on material aspects of lossy ceramics in the sub-terahertz-to-terahertz range and careful choice of ceramic materials with desirable vacuum, thermal, mechanical and charging properties.

According to (1), highly efficient mode selection can be achieved in advanced gyrotron cavities characterized by a reduced effective cavity length  $L_1$  of the competing modes. This is because the ratio  $I_1/I_2$  of starting currents of the competing and operating modes is proportional to the second power of  $L_2/L_1$ . Moreover, a decrease in effective cavity length of the competing modes greatly reduces their diffractive quality factors [5], thereby making an additional contribution to the rise in  $I_1/I_2$ . Such an improved selectivity can be realized in advanced gyrotron cavities with abrupt structural variations, which have little or no effect on the operating mode (or mode pair), but initiates reflection of the competing modes. Among such cavities are complex cavities [24, 25], cavities with transverse (circumferential) selective grooves [10], coaxial cavities with stepped inner conductors [8], and cavities with coaxial inserts partially coated by dielectrics [9]. Contrary to conventional cylindrical cavities, these cavities, however, can exhibit unwanted conversion between coupled radial modes due to abrupt change of the longitudinal (axial) structure. Even though such mode conversion is well-studied in cold cavities [26-30], its effect on the beam interaction with first- and second-harmonic modes still remains poorly explored [31] and therefore may present a hidden factor in designing the advanced cavities for second-harmonic gyrotrons.

A fundamentally different method of mode selection can be employed in cylindrical gyrotron cavities with mode-converting longitudinal corrugations [32], which also find use in coaxial cavities of the first-harmonic gyrotrons [33-36]. Such wall corrugations have generally only a slight effect on the operating mode of a second-harmonic gyrotron, provided that the corrugation depth equals half its wavelength. This depth corresponds to nearly a quarter wavelength of the competing first-harmonic modes. Under this condition, the first-harmonic modes suffer from conversion to coupled azimuthal modes (Bloch harmonics) [37, 38]. If the number of corrugations is large enough, high-order Bloch harmonics feature caustic radii far in excess of the beam radius. In this case, one might expect the reduction of the beam-wave coupling coefficients  $C_{l,1}^2$  for the first-harmonic competing modes due to mode-converting corrugations [32, 36] and, consequently, the rise in the ratio  $I_1/I_2$  of starting currents of the first- and second-harmonic modes (see (1)). Thus mode-converting wall corrugations are expected to improve mode selection in cavities of second-harmonic gyrotrons as suggested by cold cavity analysis (without electron beam) [32]. However, before proceeding to a concrete design of such a cavity, it is necessary to develop a self-consistent theory of the beam-wave interaction in a gyrotron cavity with mode-converting corrugations and to investigate the influence of corrugations with half- and quarter-wavelength depth on the starting currents of the cavity modes. Such an investigation is the prime object of this study.

## 2. Gyrotron equations

Consider a gyrotron cavity with  $N$  longitudinal wedge-shaped wall corrugations of the depth  $d$  and width  $w = \varphi_L R$  (Fig. 1). We neglect conversion of radial cavity modes due to slow variation of the cavity radius  $R(z)$  [26-30], and first assume that the cavity is made of a perfect electric conductor. Such a corrugated cavity supports pure TE modes ( $E_z = 0$ ). In the cylindrical coordinates  $\{r, \varphi, z\}$ , their fields can be written as

$$B_z = k_{\perp}^2 V(z) \Psi(r, \varphi) \exp(-i\omega t), \quad E_{\varphi} = -ikV(z) \frac{\partial \Psi(r, \varphi)}{\partial r} \exp(-i\omega t), \quad (2)$$

where  $V(z)$ ,  $k_{\perp}$  and  $\omega$  are the mode amplitude, transverse wavenumber and angular frequency, respectively,  $\Psi(r, \varphi)$  is the membrane function, which can be expanded in terms of Bloch harmonics  $\Psi = \sum_{n=-\infty}^{\infty} A_n J_{k_n}(k_{\perp} r) \exp(ik_n \varphi)$  inside the guiding channel  $0 \leq r \leq R$  (region I) and Fourier harmonics  $\Psi = \sum_{l=0}^{\infty} X_l \left[ J_{\xi_l}(k_{\perp} r) - N_{\xi_l}(k_{\perp} r) J'_{\xi_l}(k_{\perp} R_d) / N'_{\xi_l}(k_{\perp} R_d) \right] \cos[\xi_l(\varphi + \varphi_L/2)]$  inside the corrugations  $R \leq r \leq R_d$  (region II), where  $k_n = m + nN$  are the azimuthal indices of the fundamental ( $n = 0$ ) and higher-order ( $n \neq 0$ ) Bloch harmonics,  $n = 0, \pm 1, \pm 2, \dots$ ,  $R_d = R + d$ ,  $\xi_l = \pi l / \varphi_L$ ,  $J_l(\cdot)$  and  $N_l(\cdot)$  are the  $l$ -th order Bessel and Neumann functions, respectively. Such field representation is known as spatial harmonic method (SHM) [37-41].

The field components (2) must satisfy continuity conditions at the interfaces between regions I and II, and boundary conditions at the perfectly conducting surface of the cavity. Using these conditions and the orthogonal properties of Bloch and Fourier harmonics, one obtains the dispersion relation for a gyrotron cavity with longitudinal wedge-shaped corrugations [37]. This equation yields real eigenvalues  $\chi = k_{\perp} R$  of TE modes of the perfectly conducting cavity. In the case of finite wall conductivity  $\sigma$ , the transverse wavenumbers of these modes becomes complex  $k_{\perp} R = \chi(1 - i/(2Q_{ohm}))$

and can be found by the perturbation technique [32, 38, 41]. Note that generally TE modes of a corrugated gyrotron cavity are in the form of coupled Bloch and Fourier harmonics. The coupling between spatial harmonics becomes weak for large number  $N$  of corrugations. In this case, the contribution from high-order harmonics to the membrane function can be neglected and one is led to an approximation called the surface impedance model (SIM) [19, 22, 42-44].

Let us next consider a helical electron beam, which propagates along the corrugated cavity from the input end ( $z = 0$ ) and interacts with a single cavity TE mode. Using a widely accepted technique, one can derive the self-consistent system of ordinary differential equations known as single-mode gyrotron equations [45, 46], which combine the wave equation for the amplitude  $V(z)$  of the cavity mode, which is excited by the electron beam, with the equations of electron motion in the mode field and axial external magnetic field  $B_0$ . In the case of a gyrotron cavity with longitudinal corrugations, these equations can be written in the following dimensionless form:

$$\begin{cases} \left( \frac{\partial^2}{\partial \zeta^2} + \delta^2 \right) f(\zeta) = I_0 \sum_{n=-\infty}^{\infty} C_{n,s} (k_{\perp}/k)^s \langle p^s \exp(i(s-n)\Psi_0) \rangle \\ \frac{dp}{d\zeta} = ip \frac{\gamma}{\gamma_0} \frac{2}{\beta_{\perp 0}^2} \frac{\omega - s\omega_c}{s\omega} - i \frac{\gamma}{\gamma_0} f(\zeta) (p^*)^{s-1} \sum_{n=-\infty}^{\infty} C_{n,s} (k_{\perp}/k)^s \exp(i(n-s)\Psi_0) \end{cases} \quad (3)$$

where  $\zeta = zG$  is the dimensionless axial coordinate,  $G = k\alpha\beta_{\perp 0}/2$ ,  $\alpha = \beta_{\perp 0}/\beta_{z0}$  is the pitch factor,  $\beta_{\perp 0} = v_{\perp 0}/c$ ,  $\beta_{z0} = v_{z0}/c$ ,  $\mathbf{v}_0 = \mathbf{p}_0/(m_e\gamma_0)$  is the initial electron velocity,  $k = \omega/c$ ,  $\delta^2 = (k^2 - k_{\perp}^2)/G^2$ ,

$f(\zeta) = -\frac{V(z)}{B_0} \frac{k^2 \beta_{\perp 0}^{s-4} \omega^{s-2} \sqrt{P}}{(s-1)! 2^{s-1} \omega_{c0}^{s-2}} \exp(-is\pi/2)$ ,  $p = p_{\perp}/p_{\perp 0} \exp(i\mathcal{G})$ ,  $p_{\perp}$  and  $\mathcal{G}$  are the transverse electron momentum and

slowly varying phase, respectively,  $I_0 = 64 \frac{I_b}{I_A} \frac{\beta_{z0}^2 \beta_{\perp 0}^{2(s-4)} \omega^{2(s-1)}}{\gamma_0 (s!)^2 2^{2s} \omega_{c0}^{2(s-1)}}$ ,  $I_b$  is the beam current,  $I_A = m_e c^3/e \approx 17$  kA,

$\omega_c = eB_0/(cm_e\gamma)$  is the electron cyclotron frequency,  $\omega_{c0} = eB_0/(cm_e\gamma_0)$ ,  $\gamma = \gamma_0 \sqrt{1 + \beta_{\perp 0}^2 (|p|^2 - 1)}$  and  $\gamma_0 = 1 + eV_b/(m_e c^2)$  is the relativistic factor and its initial value,  $V_b$  is the beam voltage,  $e$  and  $m_e$  are the electron charge and rest mass, respectively,  $\langle \dots \rangle$  denotes averaging over the beam electrons,  $C_{n,s} = \sqrt{\alpha_n J_{k_n-s}^2(k_{\perp} r_c) / (P_n (1 + P_c/P))}$  is the

coefficient of beam coupling with  $n$ -th Bloch harmonic,  $\alpha_n = |A_n|^2 P_n/P$  is the contribution of the  $n$ -th Bloch harmonic to the power flow  $P$  along the guiding channel (region I) [32],  $P_n = \chi^2 J_{k_n}^{\prime 2}(\chi) + 2\chi J_{k_n}(\chi) J_{k_n}'(\chi) + (\chi^2 - k_n^2) J_{k_n}^2(\chi)$ ,

$P = \sum_{n=-\infty}^{\infty} |A_n|^2 P_n$ ,  $\sum_{n=-\infty}^{\infty} \alpha_n = 1$ ,  $P_c = \frac{\varphi_L \chi^2}{4\varphi_S} \left( 2P_{c0} + \sum_{l=1}^{\infty} P_{cl} \right)$  is the power flow along the corrugations (region II),

$P_{cl} = |X_l|^2 \left[ B_{\xi} g_{\xi}^2(\chi R_d/R) - 2g_{\xi}(\chi) g_{\xi}'(\chi)/\chi - D_{\xi} g_{\xi}^2(\chi) - 1 \right]$ ,  $B_l = (R_d^2/R^2 - l^2/\chi^2)$ ,  $D_l = (1 - l^2/\chi^2)$ ,

$P_{c0} = |X_0|^2 \left[ B_0 g_0^2(\chi R_d/R) - D_0 g_0^2(\chi) - g_0'^2(\chi) \right]$ ,  $g_l(z) = J_l(z) - N_l(z) J_l'(\chi R_d/R) / N_l'(\chi R_d/R)$ ,  $r_c$  and  $\Psi_0$

( $0 \leq \Psi_0 < 2\pi$ ) are the polar coordinates of the electron guiding centers, respectively. Note that in order to avoid artificial coupling of the  $n$ -th and  $n'$ -th Bloch harmonics in computations, the number  $N_{\psi}$  of discretization steps along the azimuthal coordinate  $\Psi_0$  must ensure non-integer value of the ratio  $(n - n')N/N_{\psi}$  [47].

The system of equations (3) takes into account the self-consistent effect of longitudinal wall corrugations on the beam-wave interaction in a gyrotron cavity. According to [22, 32, 34, 40, 42], for a selected  $TE_{m,p}$  mode this effect is associated with the change of the complex transverse wavenumber  $k_{\perp} R = \chi(1 - i/(2Q_{ohm}))$ . More importantly, corrugations can initiate energy transformation from the  $TE_{m,p}$  mode (fundamental Bloch harmonic) to one or more  $TE_{k_n,l}$  modes (higher-order Bloch harmonics) [32]. Such energy transformation is known as mode conversion. In this process, the normalized amplitude  $\alpha_n$  decreases from unity for the fundamental ( $n = 0$ ) Bloch harmonic and increases from zero for one or more higher-order ( $n \neq 0$ ) harmonics (see [32] for more details). As the corrugation depth  $d$  (or width  $w$ ) approaches zero, one obtains  $\chi \rightarrow \mu'_{m,p}$ ,  $\alpha_0 \rightarrow 1$ ,  $\alpha_n \rightarrow 0$  ( $n \neq 0$ ),  $P_c \rightarrow 0$ ,  $P_0 = (\mu_{m,p}'^2 - m^2) J_m^2(\mu_{m,p}')$ , where  $\mu_{m,p}'$  is the  $p$ -th root of the function  $J_m'(\cdot)$ . In this case, gyrotron equations (3) take the standard form and describe beam-wave interaction in a conventional cylindrical gyrotron cavity [16, 45, 46].

Equations (3) must be supplemented by the outgoing-wave boundary conditions at the input ( $\zeta = 0$ ) and output ( $\zeta = \zeta_{out}$ ) ends of a gyrotron cavity, and the initial condition  $p(0) = \exp(i\mathcal{G}_0)$  with  $0 \leq \mathcal{G}_0 < 2\pi$  for the dimensionless electron momentum [16, 45, 46]. With the knowledge of the complex transverse wavenumbers  $k_{\perp}$  and beam-wave coupling

coefficients  $C_{n,s}^2$  for the cavity modes, these equations can be applied to find mode frequencies and starting currents, provided that the field amplitude  $f(\zeta)$  and interaction efficiency are small enough. In the next Section, we will investigate  $k_{\perp}$  and  $C_{n,s}^2$  for TE modes of a gyrotron cavity with longitudinal wedge-shaped corrugations.

### 3. Mode conversion in a corrugated cavity

As an example, let us consider the second-harmonic ( $s = 2$ ) TE<sub>6,12</sub> mode ( $\mu'_{6,12} \approx 44.35$ ) of a gyrotron cavity with longitudinal wedge-shaped corrugations (Fig. 1). We focus our attention on the main cavity section with constant radius of 0.248 cm. In the following, we consider corrugations of equal depth and width, i.e.  $w = d$ . Such a design of corrugations is usually the most appropriate with regard to cavity fabrication. The cavity is assumed to be made of copper with reduced conductivity  $\sigma = 2.9 \cdot 10^7$  S/m due to surface roughness.

Fig. 2 shows the influence of the corrugation depth  $d$  on cutoff frequency  $f_c$  and ohmic Q-value found from SHM and SIM for the TE<sub>6,12</sub> mode. In calculations, the number of corrugations is set to 60 and satisfy the condition  $N > \chi + |m| > 2|m|$ , which is the well-known extended criterion of SIM validity for a corrugated conducting rod [40]. In this case, the eigenvalue of the TE<sub>6,12</sub> mode corresponds to the twelfth root of the dispersion relation. Although the condition  $N > \chi + |m|$  holds true, there is an essential discrepancy between SHM and SIM in the vicinity of  $d = \lambda/4 \approx 0.009$  cm (see Fig. 2), where  $\lambda = c/f_c$  is the cutoff wavelength. As was shown in [37, 38], this discrepancy slowly decreases with  $N$  and is attributed to coupling between fundamental and higher-order Bloch harmonics. In a corrugated gyrotron cavity, such a mode coupling depends critically on the corrugation depth [32].

Usually the coupling between Bloch harmonics is weak, provided that the depth  $d$  is close to  $\lambda/2$  (half-wavelength) and the corrugation number  $N$  is relatively large [32]. In the case of the TE<sub>6,12</sub> mode, one obtains  $d = \lambda/2 \approx 0.019$  cm. As Fig. 2 suggests, for such a corrugation depth, the cutoff frequency of the TE<sub>6,12</sub> mode approaches 792.25 GHz and is close to that of the TE<sub>6,11</sub> mode ( $\mu'_{6,11} \approx 41.18$ ) of the smooth cylindrical cavity ( $d = 0$ ). This is because these modes have much the same field distribution inside the cavity region  $0 \leq r \leq R$  [32].

Fig. 3 shows the cutoff frequency of the TE<sub>6,12</sub> mode as a function of the number  $N$  of corrugations for  $d = \lambda/2 \approx 0.019$  cm (see the line  $\chi = \mu'_{6,11}$ ). It can be seen that this frequency deviates only slightly from 792.25 GHz, thus approximately satisfying the condition  $\chi = \mu'_{6,11}$  for any  $N$ . The exceptions are  $N = 33$  and  $N = 46$ . As can be seen from Figs. 3 and 4a, for this  $N$  the cutoff frequency  $f_c$  undergoes a change, which is attributed to conversion of the fundamental (TE<sub>6,12</sub> mode) to higher-order Bloch harmonics. In the case of  $d = \lambda/2$ , such mode conversion is also evident for  $N = 12, 6, 4, 3, 2$  and 1 (Fig. 4a). In this case, however, the wall corrugations couple the co-rotating TE<sub>+6,12</sub> and counter-rotating TE<sub>-6,12</sub> modes with identical eigenvalues and therefore have no effect on cutoff frequency of the cavity mode (Fig. 3).

As the number  $N$  of corrugations decreases and  $|k_n|$  becomes smaller than  $\chi$ , the number of higher-order Bloch harmonics (TE <sub>$k_n,l$</sub>  modes) in the vicinity of 792.25 GHz increases (Fig. 3). However, as discussed above, this fact is generally of no consequence for the selected second-harmonic TE<sub>6,12</sub> mode at  $d = \lambda/2$ . Moreover, in the following, to ensure the strongest coupling of this mode (fundamental Bloch harmonic) with the electron beam we will keep the value of  $\chi r_c / R$  constant and set the beam radius  $r_c$  close to the maximum of the function  $J_{6-2}^2(\chi r_c / R)$ , regardless of the mode eigenvalue  $\chi$ . For such beam radius, the TE <sub>$k_n,l$</sub>  modes are weakly coupled with the electron beam, provided that  $|k_n| > |m|$  ( $N > 2|m|/n$ ). This can be seen from Fig. 4b, which shows the dependence of the maximal beam-wave coupling coefficients  $C_s = \max\{C_{n,s}^2\}$  on  $N$  for the TE<sub>6,12</sub> mode (blue circles) and all other TE <sub>$k_n,l$</sub>  modes (red stars) with eigenvalues lying in the range  $|\chi - \mu'_{6,11}| < \pi/2$  (see Fig. 3). As is evident from Fig. 4b, among these modes the TE<sub>6,12</sub> mode features the strongest beam-wave coupling, which is nearly the same as for the TE<sub>6,11</sub> mode of the smooth cylindrical cavity, i.e.  $C_s \approx C_s^{(0)}$ , and slightly decreases with  $N$  due to increasing power flow  $P_c$  along the corrugations. In some cases discussed above this coupling can be additionally weakened by the mode conversion.

It is well known that for conventional cylindrical cavities with metal wall, the ohmic Q-value of the TE <sub>$m,p$</sub>  mode equals  $Q_{ohm}^{(0)} \approx R/\delta_s (1 - m^2/\mu_{m,p}^{\prime 2})$  [48], and therefore is mostly determined by the transverse dimensions of the cavity surface, where  $\delta_s$  is the skin-depth. Obviously, longitudinal wall corrugations tend to increase the conducting surface of a gyrotron cavity. Therefore, the ohmic losses in a corrugated gyrotron cavity are generally higher than those in a cylindrical cavity (Fig. 2b) and they increase with increasing number of corrugations [22, 32, 41, 43]. For the TE<sub>6,12</sub> mode, this can be seen in Fig. 5. Compared to this mode, the higher-order Bloch harmonics have lower ohmic Q-values for  $|k_n| = |m + nN| > 6$ . That is the reason why the ohmic Q-value drops off with conversion of the fundamental to the higher-order Bloch harmonics in the case

of  $N = 33$  or  $N = 46$  (Fig. 5). As shown above, for  $d = \lambda/2$  such mode conversion in a gyrotron cavity with longitudinal wall corrugations is the exception rather than the rule.

However, the situation is radically different for the corrugations with quarter-wavelength depth ( $d = \lambda/4$ ) [32]. In this case, as a rule, there are no pure  $\text{TE}_{6,12}$  and  $\text{TE}_{k_n,l}$  modes in the corrugated gyrotron cavity and the cavity modes have the form of coupled Bloch harmonics. The obvious exception is the extreme case  $N \rightarrow \infty$ , in which the mode coupling goes to zero and the results of the spatial harmonic method approach those of the SIM. In this case,  $\alpha_0 \rightarrow 1$ ,  $\alpha_n \rightarrow 0$  ( $n \neq 0$ ) and  $\chi \rightarrow \mu_{6,11}$  for  $d = \lambda/4$  [22, 37, 43], where  $\mu_{m,p}$  is the  $p$ -th root of the Bessel function  $J_m(\cdot)$  (see Fig. 2a). As a result, for  $d = \lambda/4 \approx 0.009$  cm and  $N \rightarrow \infty$  one gets the pure  $\text{TE}_{6,12}$  mode of the corrugated cavity with the cutoff frequency of 823.03 GHz ( $\chi = \mu_{6,11}$ ).

Let us next investigate coupled modes of the corrugated gyrotron cavity in the vicinity of 823.03 GHz, so that the mode eigenvalues satisfy the condition  $|\chi - \mu_{6,11}| < \pi/2$  for  $d = \lambda/4 \approx 0.009$  cm and  $m = 6$ . Fig. 6a shows the cutoff frequencies of these modes versus the number of corrugations. Again, it can be seen that the number of coupled modes increases with decreasing number of corrugations. However, contrary to our previous findings, in this case the beam-wave coupling for all these modes is not so strong as for the  $\text{TE}_{6,11}$  mode of the smooth cylindrical cavity, even though the number of corrugations is large. This is because the modes contain the higher-order Bloch harmonics, which, as compared to the fundamental harmonic, have weaker coupling with the electron beam for the selected beam radius  $r_c$ . Among them we discriminate the modes, which feature the maximal beam-wave coupling coefficients  $C_s = \max\{C_{n,s}^2\}$  for each  $N$ . Cutoff frequencies and coefficient  $C_s = \max\{C_{n,s}^2\}$  of these modes are shown in Figs. 6b and 7a, respectively.

Fig. 7b shows the effect of the corrugations with quarter-wavelength depth on the ohmic Q-values of cavity modes having the maximal beam-wave coupling coefficients for each  $N$ . Firstly, it should be noted that such corrugations lead to high ohmic losses, even though the coupling of Bloch harmonics is neglected (see Fig. 2a and [22, 32, 41, 43]). Secondly, as the mode coupling in a corrugated gyrotron cavity strengthens, it becomes more and more difficult to emerge any regular trends in the behavior of ohmic Q-values of the cavity modes, which are in the form of complex mixtures of different Bloch harmonics. At the same time, it is reasonably safe to suggest that these ohmic Q-values are generally lower than those of the  $\text{TE}_{6,12}$  mode of the corrugated gyrotron cavity for  $d = \lambda/2$  (see Fig. 5).

In the next Section, we will investigate the effect of corrugations with half- and quarter-wavelength depths on the starting currents of TE modes of the gyrotron cavity. For each type of corrugations we will consider two cases  $N = 44$  and  $N = 19$ , which correspond to relatively large and small number of corrugations, respectively. These values are shown by vertical green lines in Figs. 3-7.

#### 4. Effect of mode-converting corrugations on starting currents

Consider a second-harmonic gyrotron equipped with a corrugated copper cavity (Fig. 1). The beam parameters are  $\alpha = 1.2$ ,  $V_b = 30$  kV and  $I_b = 0.5$  A. In the absence of corrugations, the gyrotron operates in the  $\text{TE}_{6,11}$  mode at the frequency of about 792.3 GHz. For this mode, the field distribution across the cavity is shown in Fig. 8a.

Fig. 9a shows the starting current  $I_{st}$  of the operating mode as a function of the magnetic field  $B_0$ . It can be seen that the starting current lies below the operating beam current in the range between 14.88 T and 15.05 T, thus offering the prospect for continuous frequency tuning with the bandwidth of 0.5 GHz.

For  $N = 44$  and  $N = 19$  the influence of the longitudinal wall corrugations with half-wavelength depth on the starting current can be also seen from Fig. 9a. As this figure suggests, such corrugations initiate slight increase of the starting current of the operating mode. This effect is stronger for larger number of corrugations and is attributed to increased power  $P_c$  and ohmic losses in the corrugated cavity (see Figs. 4b and 5). The increased ohmic losses due to corrugations would thus be expected to reduce the beam-wave interaction efficiency and output power of the gyrotron [16]. Note that in the case of  $d = \lambda/2$  the coupling between Bloch harmonics is extremely weak for both  $N = 19$  and  $N = 44$ . In this case, the gyrotron operating mode is nearly the pure  $\text{TE}_{6,12}$  mode of the corrugated cavity (Fig. 8b), while the nearby  $\text{TE}_{k_n,l}$  modes have high starting currents owing to extremely weak coupling with the electron beam (Fig. 4b).

As discussed earlier, this is not the case for a corrugated cavity with quarter-wavelength depth of the corrugations. In this cavity, the cavity modes are composed of coupled Bloch harmonics. Fig. 9b shows the starting currents of these modes versus  $B_0$  for  $N = 19, 44$  and 60. Comparison of Figs. 9a and 9b indicates that the corrugations with quarter-wavelength depth initiate a distinct increase of the starting current due to combined effect of mode conversion and ohmic losses. For  $N = 60$  and  $N = 44$ , such an increase amounts to about 63% and 392% of the starting current of the  $\text{TE}_{6,11}$  mode of the smooth gyrotron cavity. In the case of  $N = 19$ , there are two modes with starting currents, which are relatively close to the operating beam current. For these modes, which are mixtures of coupled Bloch harmonics (Fig. 8c), the minimum starting currents are higher than that of the  $\text{TE}_{6,11}$  mode of the smooth gyrotron cavity by a factor of 6.8 and 13.7. As a result, in the case of corrugated cavity with quarter-wavelength deep corrugations, the coupled modes can satisfy the oscillation condition  $I_{st} < I_b$  only marginally for  $N = 60$  and fail to meet this condition for  $N = 19$  and  $N = 44$ , regardless of the magnetic field

$B_0$ . This feature differentiates corrugations with quarter-wavelength depth from those with half-wavelength depth and can be applied for mode selection in the cavities of second-harmonic gyrotrons.

For such mode selection the gyrotron cavity should incorporate wall corrugations with half-wavelength depth, which has a slight effect on the second-harmonic operating mode. By contrast, in this case, the first-harmonic competing modes are subject to the condition  $d \approx \lambda/4$  and therefore would exhibit mode conversion and increased ohmic losses, which tend to increase their starting currents (see (1)). In addition, the frequencies of these modes change with the number of corrugations. Therefore, with properly-selected  $N$ , one might expect to achieve favorable conditions for selective suppression of the most dangerous first-harmonic modes at moderately increased ohmic losses of the operating mode. Further investigation will be aimed at examining the performance of mode-converting corrugations by the concrete example of a corrugated cavity for a sub-terahertz second-harmonic gyrotron.

Finally, it should be mentioned that longitudinal wall corrugations can increase the risk of mode conversion between radial modes in tapered sections of the gyrotron cavity. It is believed that this unwanted phenomenon can affect the field pattern of outgoing radiation, but is of little or no consequence for beam-wave interaction in the cavity [49]. In gyrotron design, this fact must be kept in mind in designing the output system, including the transition from the corrugated cylindrical cavity to a smooth-wall output waveguide.

#### 4. Conclusion

Self-consistent single-mode gyrotron equations have been derived for gyrotrons with cylindrical cavities incorporating an arbitrary number of periodic longitudinal wall corrugations. For modes of the corrugated cavity, the eigenvalues, ohmic losses and beam-wave coupling coefficients have been investigated with respect to the corrugation parameters. Using these characteristics, the gyrotron equations have been applied to investigate the effect of corrugations on electron beam interaction with cavity modes. In the general case, these modes appear as superposition of different azimuthal harmonics with mutual coupling, which depends critically on the corrugation depth. For corrugations with half-wavelength depth, this coupling has been shown to be generally weak, even though the spectrum of azimuthal harmonics becomes denser with decreasing number of corrugations. In this case, azimuthal harmonics behave much like TE modes of a smooth cylindrical cavity. Therefore, in the corrugated gyrotron cavity, the complex transverse wavenumbers and beam-wave coupling coefficients of cavity modes are found to be little affected by corrugations with half-wavelength depth. As a result, such corrugations have been shown to initiate only a slight increase of the mode starting currents due to ohmic wall losses, which decrease with decreasing number of corrugations. By contrast, in the corrugated gyrotron cavity with quarter-wavelength deep corrugations, the coupling of different azimuthal harmonics is strong and cannot be ignored, even though the number of corrugations is large. This coupling strongly affects the eigenvalues of cavity modes. Moreover, it has been found that it weakens the beam-wave coupling in the corrugated cavity. For this reason, it has been shown that mode-converting corrugations are capable of providing several-fold increase in starting currents for cavity modes with frequencies, which correspond to a quarter-wavelength approaching the corrugation depth. Such mode discrimination by means of beam-wave coupling coefficients has been demonstrated with a purely electrodynamic method, as opposed to that provided by electron-optical methods of [4, 7]. In advanced cavities with improved mode selection for second-harmonic gyrotrons, mode converting corrugations can be used in combination with non-uniform coaxial inserts [8, 9] to provide simultaneous reduction of effective cavity lengths, total quality factors, and beam-wave coupling coefficients of competing modes (see (1)).

**Acknowledgements** The work of Vitalii I. Shcherbinin was supported by a Georg Forster Research Fellowship for Experienced Researchers from the Alexander von Humboldt Foundation.

#### References

- 1) E.A. Nanni, A.B. Barnes, R.G. Griffin, R.J. Temkin, IEEE Trans. Terahertz Sci. Technol. (2011) <https://doi.org/10.1109/TTHZ.2011.2159546>
- 2) M.Y. Glyavin, T. Idehara, S.P. Sabchevski, IEEE Trans. THz Sci. Technol. (2015) <https://doi.org/10.1109/TTHZ.2015.2442836>
- 3) M.K. Hornstein, V.S. Bajaj, R.G. Griffin, K.E. Kreisler, I. Mastovsky, M.A. Shapiro, J.R. Sirigiri, R.J. Temkin, IEEE Trans. Electron Devices (2005) <https://doi.org/10.1109/TED.2005.845818>
- 4) V.L. Bratman, Yu.K. Kalynov, V.N. Manuilov, Phys. Rev. Lett. (2009) <https://doi.org/10.1103/PhysRevLett.102.245101>
- 5) Y.J. Huang, L.H. Yeh, K.R. Chu, Phys. Plasmas (2014) <https://doi.org/10.1063/1.4900415>
- 6) S.H. Kao, C.C. Chiu, K.R. Chu, Phys. Plasmas (2012) <https://doi.org/10.1063/1.3684663>
- 7) N.S. Ginzburg, M.Y. Glyavin, A.M. Malkin, V.N. Manuilov, R.M. Rozental, A.S. Sedov, A.S. Sergeev, V.Y. Zaslavsky, I.V. Zotova, T. Idehara, IEEE Trans. Plasma Sci. (2016) <https://doi.org/10.1109/TPS.2016.2585307>
- 8) V.I. Shcherbinin, V.I. Tkachenko, K.A. Avramidis, J. Jelonnek, IEEE Trans. Electron Devices (2019) <https://doi.org/10.1109/TED.2019.2944647>
- 9) V.I. Shcherbinin, Y.K. Moskvitina, K.A. Avramidis, J. Jelonnek, IEEE Trans. Electron Devices (2020) <https://doi.org/10.1109/TED.2020.2996179>

- 10) I.V. Bandurkin, A.P. Fokin, M.Y. Glyavin, A.G. Luchinin, I.V. Osharin, A.V. Saviolov, IEEE Electron Device Lett. (2020) <https://doi.org/10.1109/LED.2020.3010445>
- 11) V.I. Shcherbinin, K.A. Avramidis, M. Thumm, J. Jelonnek, J. Infrared Millim. Terahertz Waves, 2020 (accepted)
- 12) La Agusu, T. Idehara, H. Mori, T. Saito, I. Ogawa, S. Mitsudo, Int. J. Infrared Millim. Waves (2007) <https://doi.org/10.1007/s10762-007-9215-y>
- 13) A.C. Torrezan, S.T. Han, I. Mastovsky, M.A. Shapiro, J.R. Sirigiri, R.J. Temkin, A.B. Barnes, R.G. Griffin, IEEE Trans. Plasma Sci. (2010) <https://doi.org/10.1109/TPS.2010.2046617>
- 14) V.I. Shcherbinin, T.I. Tkachova, V.I. Tkachenko, IEEE Trans. Electron Devices (2018) <https://doi.org/10.1109/TED.2017.2769219>
- 15) S.K. Jawa, R.G. Griffin, I.A. Mastovsky, M.A. Shapiro, R.J. Temkin, IEEE Trans. Electron Devices (2020) <https://doi.org/10.1109/TED.2019.2953658>
- 16) V.I. Shcherbinin, A.V. Hlushchenko, A.V. Maksimenko, V.I. Tkachenko, IEEE Trans. Electron Devices (2017) <https://doi.org/10.1109/TED.2017.2730252>
- 17) S. Spira-Hakkarainen, K.E. Kreischer, R.J. Temkin, IEEE Trans. Plasma Sci. (1990) <https://doi.org/10.1109/27.55903>
- 18) K.D. Hong, G.F. Brand, T. Idehara, J. Appl. Phys. (1993) <https://doi.org/10.1063/1.354265>
- 19) K.A. Avramides, C.T. Iatrou, J.L. Vomvoridis, IEEE Trans. Plasma Sci. (2004) <https://doi.org/10.1109/TPS.2004.828781>
- 20) Yu.S. Oparina, A.V. Saviolov, J. Infrared Millim. Terahertz Waves (2018) <https://doi.org/10.1007/s10762-018-0499-x>
- 21) V.I. Shcherbinin, G.I. Zaginaylov, V.I. Tkachenko, Problems Atomic Sci. Technol. 6 (106), 255 (2016)
- 22) V.I. Shcherbinin, V.I. Tkachenko, J. Infrared Millim. Terahertz Waves (2017) <https://doi.org/10.1007/s10762-017-0386-x>
- 23) K.A. Avramides, J.L. Vomvoridis, C.T. Iatrou, AIP Conference Proceedings (2006) <https://doi.org/10.1063/1.2158787>
- 24) Q. Zhao, S. Yu, T. Zhang, IEEE Trans. Electron Devices (2017) <https://doi.org/10.1109/TED.2017.2756635>
- 25) M.M. Melnikova, A.G. Rozhnev, N.M. Ryskin, Y. Tatematsu, M. Fukunari, Y. Yamaguchi, T. Saito, IEEE Trans. Electron Devices (2017) <https://doi.org/10.1109/TED.2017.2764874>
- 26) O. Dumbrajs, E. Borie, Int. J. Electron. (1988) <https://doi.org/10.1080/00207218808945230>
- 27) D. Wagner, G. Gantenbein, W. Kasperek, M. Thumm, Int. J. Infrared Millim. Waves (1995) <https://doi.org/10.1007/BF02274811>
- 28) G.I. Zaginaylov, V.I. Shcherbinin, K. Schünemann, M.Yu. Glyavin, Proc. 8th MSMW (2013) <https://doi.org/10.1109/MSMW.2013.6622127>
- 29) A.V. Maksimenko, G.I. Zaginaylov, V.I. Shcherbinin, Physics of Particles and Nuclei Letters (2015) <https://doi.org/10.1134/S1547477115020168>
- 30) A.V. Maksimenko, V.I. Shcherbinin, V.I. Tkachenko, J. Infrared Millim. Terahertz Waves (2019) <https://doi.org/10.1007/s10762-019-00589-x>
- 31) A.V. Maksimenko, V.I. Shcherbinin, A.V. Hlushchenko, V.I. Tkachenko, K.A. Avramidis, J. Jelonnek, IEEE Trans. Electron Devices (2019) <https://doi.org/10.1109/TED.2019.2893888>
- 32) T.I. Tkachova, V.I. Shcherbinin, V.I. Tkachenko, J. Infrared Millim. Terahertz Waves (2019) <https://doi.org/10.1007/s10762-019-00623-y>
- 33) V.A. Flyagin, V.I. Khizhnyak, V.N. Manuilov, M.A. Moiseev, A.B. Pavelyev, V.E. Zapevalov, N.A. Zavolsky, Int. J. Infrared Millim. Waves (2003) <https://doi.org/10.1023/A:1021667030616>
- 34) S.P. Savaidis, Z.C. Ioannidis, N.A. Stathopoulos, IEEE Trans. Microwave Theory Tech. (2012) <https://doi.org/10.1109/TMTT.2012.2209440>
- 35) Z.C. Ioannidis, K.A. Avramidis, I.G. Tigelis, J. Infrared Millim. Terahertz Waves (2015) <https://doi.org/10.1007/s10762-015-0152-x>
- 36) Z.C. Ioannidis, K.A. Avramidis, I.G. Tigelis, IEEE Trans. Electron Devices (2016) <https://doi.org/10.1109/TED.2016.2518217>
- 37) T.I. Tkachova, V.I. Shcherbinin, V.I. Tkachenko, Proc. Int. Conf. Math. Methods Electromagn. Theory (2018) <https://doi.org/10.1109/MMET.2018.8460433>
- 38) T.I. Tkachova, V.I. Shcherbinin, V.I. Tkachenko, Problems Atomic Sci. Technol. 6 (118), 67 (2018)
- 39) Z.C. Ioannidis, O. Dumbrajs, I.G. Tigelis, IEEE Trans. Plasma Sci. (2006) <https://doi.org/10.1109/TPS.2006.876518>
- 40) Z.C. Ioannidis, K.A. Avramides, G.P. Latsas, I.G. Tigelis, IEEE Trans. Plasma Sci. (2011) <https://doi.org/10.1109/TPS.2011.2118766>
- 41) T.I. Tkachova, V.I. Shcherbinin, V.I. Tkachenko, Problems Atomic Sci. Technol. 4 (122), 31 (2019)
- 42) C.T. Iatrou, S. Kern, A.B. Pavelyev, IEEE Trans. Microw. Theory Techn. (1996) <https://doi.org/10.1109/22.481385>
- 43) V.I. Shcherbinin, B.A. Kochetov, A.V. Hlushchenko, V.I. Tkachenko, IEEE Trans. Microw. Theory Techn. (2019) <https://doi.org/10.1109/TMTT.2018.2882493>
- 44) V.I. Shcherbinin, V.I. Fesenko, T.I. Tkachova, V.R. Tuz, Phys. Rev. Applied (2020) <https://doi.org/10.1103/PhysRevApplied.13.024081>
- 45) V.L. Bratman, M.A. Moiseev, M.I. Petelin, R.É. Érm, Radiophys. Quantum Electron. (1973) <https://doi.org/10.1007/BF01030898>
- 46) V.A. Flyagin, A.V. Gaponov, M.I. Petelin, V.K. Yulpatov, IEEE Trans. Microwave Theory Tech. (1977) <https://doi.org/10.1109/TMTT.1977.1129149>

- 47) S. Kern, K.A. Avramides, M.H. Beringer, O. Dumbrajs, Y. Liu, Proc. Int. Conf. Infrared Millim. Terahertz Waves (2008) <https://doi.org/10.1109/ICIMW.2008.4665584>
- 48) S.N. Vlasov, L.I. Zagryadskaya, M.I. Petelin, Radiophys. Quantum Electron. (1973) <https://doi.org/10.1007/BF01080919>
- 49) A.V. Maksimenko, V.I. Shcherbinin, V.I. Tkachenko, Proc. IEEE Ukrainian Microwave Week (2020) <https://doi.org/10.1109/UkrMW49653.2020.9252719>

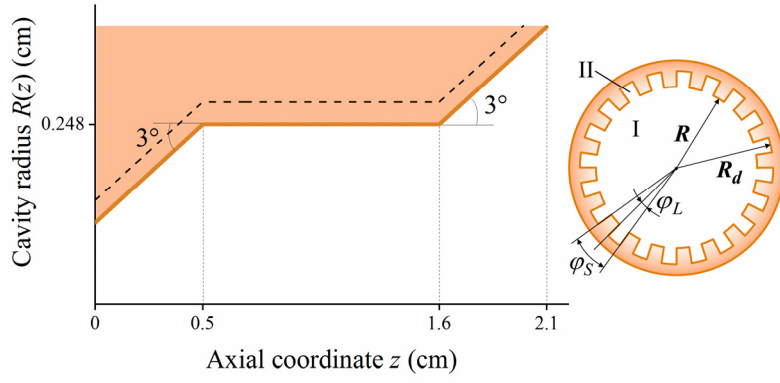


**Fig. 1** Structure of a corrugated cylindrical cavity

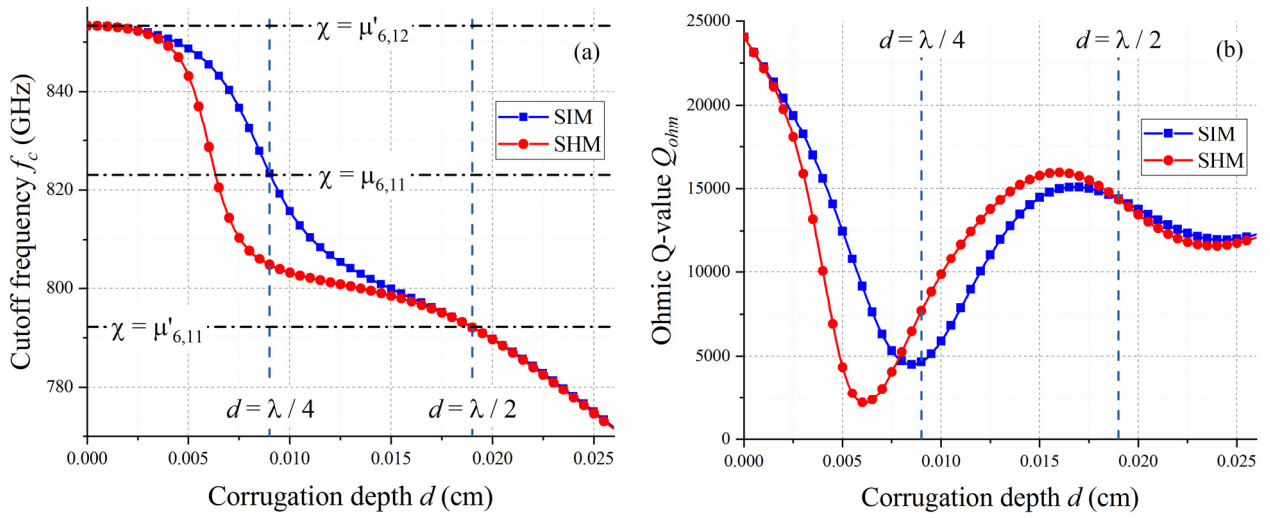


**Fig. 2** (a) Cutoff frequency  $f_c = c\chi/(2\pi R)$  and (b) ohmic Q-value of a cylindrical waveguide with longitudinal corrugations versus the corrugation depth  $d$  ( $R = 0.248$  cm,  $N = 60$ )

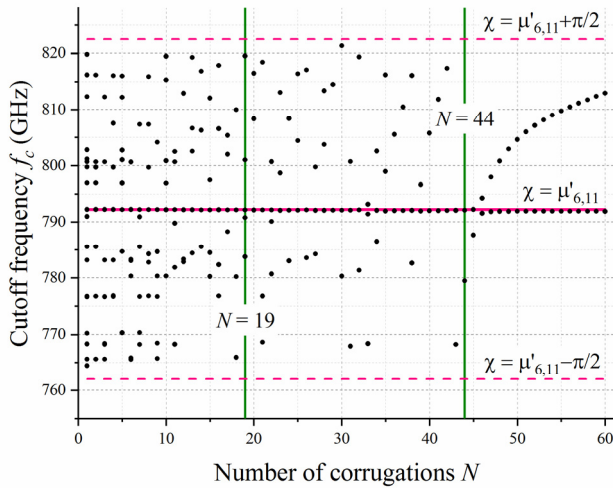


**Fig. 3** Cutoff frequencies of the corrugated cylindrical waveguide versus the number of corrugations for  $d = \lambda/2 \approx 0.019$  cm ( $m = 6$ ,  $R = 0.248$  cm)

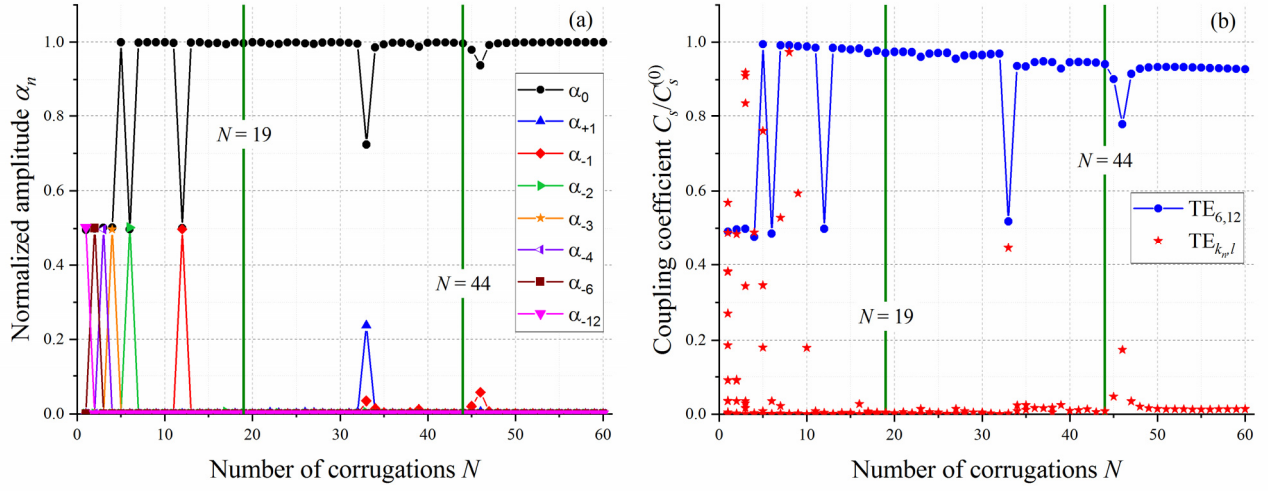


**Fig. 4** (a) Normalized amplitudes  $\alpha_n$  of the  $n$ -th Bloch harmonics for the  $TE_{6,12}$  mode and (b) normalized maximal coefficients  $C_s/C_s^{(0)}$  of the beam-wave coupling for the  $TE_{6,12}$  and  $TE_{k_p,l}$  modes versus  $N$ , where  $C_s$  equals  $C_s^{(0)}$  for  $d = 0$  ( $R = 0.248$  cm,  $d = \lambda/2 \approx 0.019$  cm,  $\chi r_c/R = const$ )

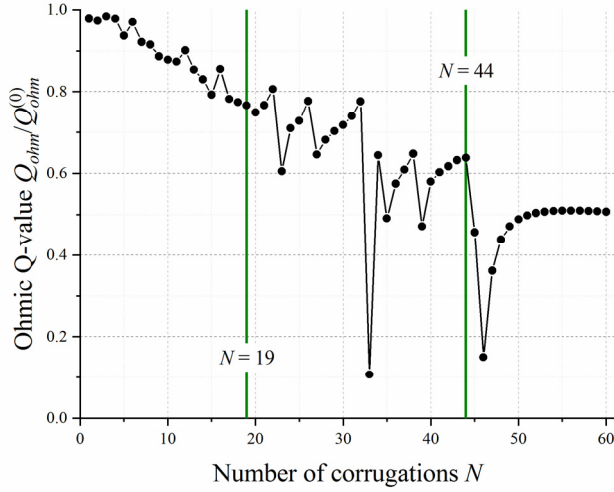


**Fig. 5** Normalized ohmic Q-value of the  $TE_{6,12}$  mode versus the number of corrugations for  $d = \lambda/2 \approx 0.019$  cm ( $R = 0.248$  cm)

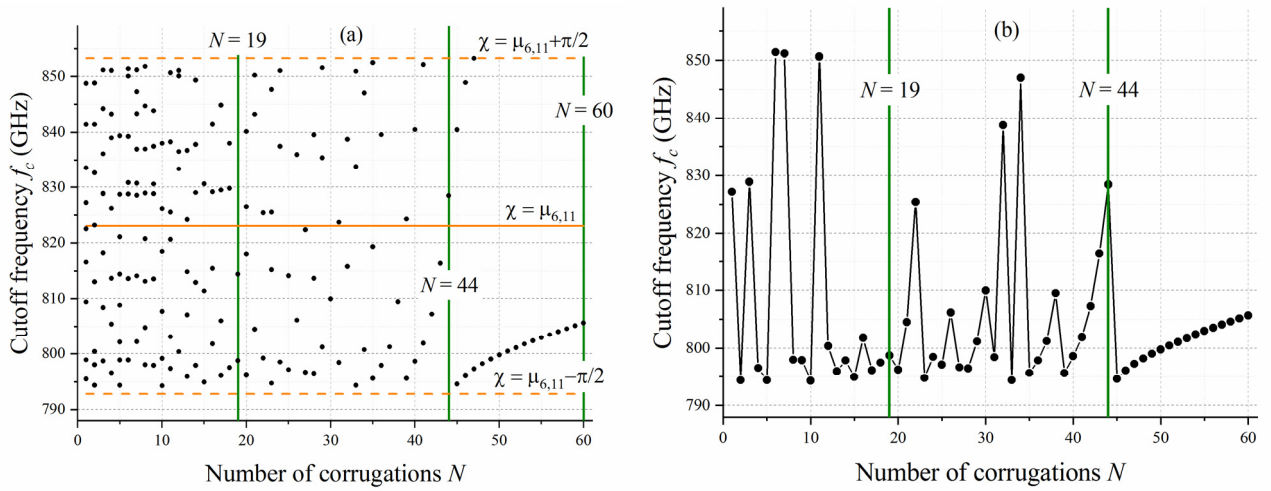


**Fig. 6** (a) The same as in Fig. 3, but for  $d = \lambda/4 \approx 0.009$  cm, and (b) cutoff frequencies of cavity modes characterized by maximal beam-wave coupling coefficients for each  $N$

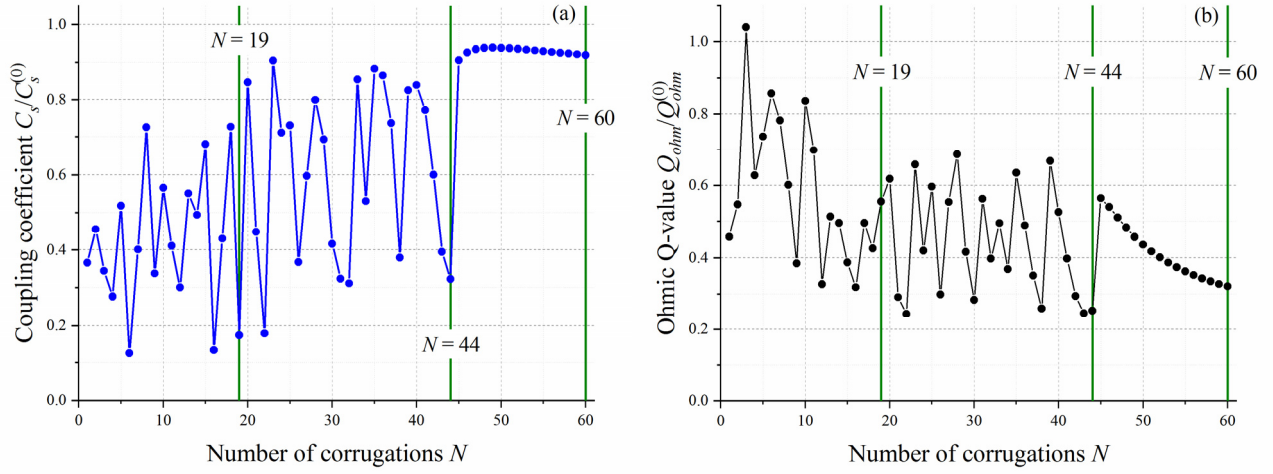


**Fig. 7** (a) Normalized beam-wave coupling coefficient  $C_s = \max\{C_{n,s}^2\}$  and (b) ohmic Q-values versus  $N$  for cavity modes depicted in Fig. 6b ( $m = 6$ ,  $R = 0.248$  cm,  $d = \lambda/4 \approx 0.009$  cm)

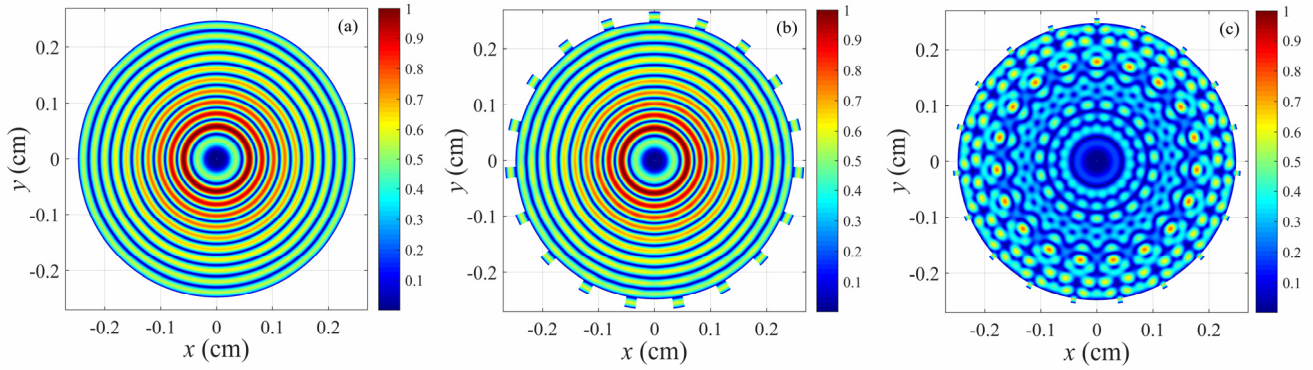


**Fig. 8** Distribution of azimuthal electric field  $|E_\varphi|$  for (a) the  $TE_{6,11}$  mode of the smooth cavity, (b) and (c) modes of the corrugated cavity with 19 wedge-shaped corrugations of half- and quarter-wavelength depth, respectively ( $R = 0.248$  cm)

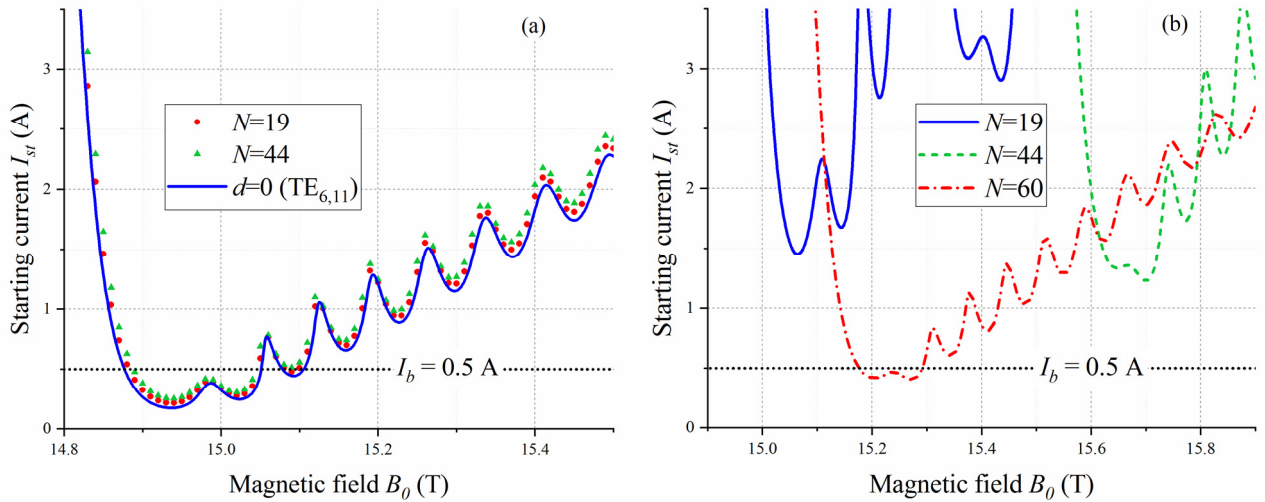


**Fig. 9** Starting currents of modes in the cylindrical gyrotron cavity with wedge-shaped corrugations of (a) half- and (b) quarter-wavelength depth